Proceedings of ICAPP 2020
15-19 March 2020 – Abu Dhabi (UAE)
SAND2019-15380C

Using Alkaline Carbonate to Mitigate Molten Corium in Severe Nuclear Reactor Accidents

David L.Y. Louie, Yifeng Wang, Rekha Rao, Alec Kucala and Jessica Kruichak
Sandia National Laboratories
1515 Eubank SE, Albuquerque, NM 87123 USA
Tel:1(505)284-5353, Fax:1(505)844-2829, Email: dllouie@sandia.gov

Abstract – *To mitigate adverse effects from molten corium following a reactor pressure vessel failure (RPVF), some new reactor designs employ a core catcher and a sacrificial material (SM), such as ceramic or concrete, to stabilize the molten corium and avoid the breach of the containment. However, existing reactors cannot be easily modified to include these SMs but could be modified to allow injectable cooling materials (current designs are limited to water). The SM proposed is based on granular carbonate minerals that can be used in existing light water reactor plants. This new SM will induce an endothermic reaction to quickly freeze the corium in place. Corium spreading is a complex process strongly influenced by coupled chemical reactions (with underlying containment material and especially with the proposed SM), including decay heat and phase change. This project focused on two research areas: experiments to demonstrate the feasibility of the novel SM concept, and modeling activities to determine the potential applications of the concept to actual nuclear plants. We have demonstrated small-scale to large-scaled experiments using lead oxide (PbO) as surrogate for molten corium which showed that the reaction of the SM with molten PbO results in a fast solidification of the melt and the formation of open pore structures in the solidified PbO because of CO_2 released from the carbonate decomposition. A simplified carbonate decomposition model has been developed to predict thermal decomposition of carbonate mineral in contact with corium. This model has been incorporated into an input model for the MELCOR code. A full-plant MELCOR simulation suggests that ex-vessel accident progression, e.g., core-concrete interaction and core spreading on the containment floor, could be significantly delayed by the introduction of SM to the reactor cavity prior to RPVF. Delays of one-half day are suggested with limited SM. Filling the cavity with SM might delay progression by day.*

I. INTRODUCTION

In a severe reactor accident, the last barrier to the release of radioactive material is the containment structure. When a containment is breached, radioactive material releases to the environment impacting the ecosystem. This is a primary concern in severe accident management [1]. Futuristic designs of nuclear reactors include sacrificial materials (SM) to provide cooling, immobilize core melt, minimize hydrogen gas production, and maximize radionuclide retention. Some new reactor designs employ a core catcher and SM (e.g., ceramic and concrete slab) to slow the molten flow [2]. Because existing reactors cannot easily be modified to include these SMs, an injectable SM delivery system could serve better.

As a part of a three-year laboratory directed research development (LDRD) project, a research study is being conducted at Sandia National Laboratories (Sandia) to develop an injectable mitigation system (IMS) to use the highly endothermic decomposition of granular alkaline carbonate (MCO3) materials to absorb decay heat and the sensible heat of the corium [3]. This study includes two parts: Part 1 demonstrates this concept in series of surrogate experiments. Part 2 uses the Sierra engineering modeling tool developed at Sandia to model the surrogate experiments as well as molten corium spreading experiments reported in the literature. In Part 2, the proposed concept feature is also evaluated using MELCOR, a U.S. Nuclear Regulatory Commission severe accident code developed at Sandia.

In this paper, we first discuss the use of MCO3 SM as a cooling medium to mitigate molten corium and the needs of these SM for deploying to current U.S. nuclear power plants. Second, the MCO3 decomposition model is discussed. Third, we briefly discuss our experimental effort by using a surrogate corium (PbO) onto a MCO3 bed. We also describe our modeling effort to using a computational fluid dynamic (CFD) code to model the experiment. Next, we discuss our modeling effort on applying this IMS to a full plant

Sandia National Laboratories is a multimission laboratory managed and operated by National Technology & Engineering Solutions of Sandia, LLC, a wholly owned subsidiary of Honeywell International Inc., for the U.S. Department of Energy's National Nuclear Security Administration under contract DE-NA0003525.

simulation for a severe accident. Finally, we provide a conclusion.

II. ALKALINE CARBONATE SM

The idea under consideration for use in the IMS is to use the principle of endothermic decomposition of alkaline carbonates (MCO3) to absorb the thermal energy (sensible and decay heat) of the molten corium to solidify its molten form. This energy effect leads to a direct cooling of the melt material. Table I shows the typical cooling values of cooling medium considered. As shown in this table, the cooling medium considered is water and alkaline carbonate. The minimum reaction temperature is also shown. For water, the transition temperature of 373 K is used from liquid to gas phase (steam). For the carbonates, the temperature values are the typical decomposition temperatures. The last three columns of this table show the cooling value in terms of energy per unit of mole, ml, and g, respectively. As shown in the energy per mole basis, $CaCO_3$ has the highest value, which is more than four times larger than water. $MgCO_3$ is less than half of the $CaCO_3$. However, the decomposition temperature for $CaCO_3$ is about twice that of the $MgCO_3$. Per mass basis, water is better than carbonate because its molecular weight is the lightest in comparison. In terms of per volume basis, all carbonates are larger than the water. Beside the density, the difference in the heat capacity is very small [3]. Based on this table, the use of the carbonate to cool a reactor accident when decay heat is significantly better than that of the water per mole or volume basis.

TABLE I

Typical cooling values of MCO_3 and water [3]

Cooling medium*	Temp. (°K)	Cooling value		
		kJ/mole	kJ/ml	kJ/g
H^2O: liquid phase to gas phase	373	40.7	2.3	2.3
$MgCO_3 \rightarrow MgO+CO_2$	623	100.7	3.6	1.2
$CaCO_3 \rightarrow CaO+CO_2$	1100	179.2	5.0	1.8

II.A. Estimation of MCO3 Needs

This section describes the use of the endothermic decomposition of the MCO3 to cool molten corium. As previously described, one of the applications for this capability is for the current operating plants. To do this, we evaluated all six types of light water reactors (LWRs) in the United States, which include pressurized water reactors (PWRs) and boiling water reactors (BWRs). A simple calculation was conducted to show the compromising amount of $CaCO_3$ required to maintain a containment pressure in a full-core RPVF accident below the best-estimate containment failure pressure (see Table II). This calculation assumes no normal leakage and heat loss to the surrounding structures during the accident. Decay heat was not considered. The details of these calculations are found in [3].

TABLE II

Calculated final containment pressures from CO_2 buildup from $CaCO_3$ decomposition [3]

Containment Type	$CaCO_3$		CO_2 (kg)	Pressures Final/Design* (kPa)
	Cavity (kg)	Consumed (mol)		
PWR				
Large dry	40,000	5.04E+4	2,219	362.5/1040
Sub-atm	60,000	2.66E+3	1161	358.0/800
Ice-condenser	75,000	6.35E+4	2796	368.8/400
BWR				
Mark I	280,000	2.83E+5	12,440	802.1/1000
Mark II	250,000	1.03E+5	4,529	466.4/1000
Mark III	350,000	6.25E+4	2,749	370.5/380

*Ultimate value [3]

II.B. Injectable Mitigation System (IMS)

To deploy the IMS, the granular IMS must be injected into the cavity in the PWR or the pedestal volume in the BWR (see Fig. 1 and Fig. 2, respectively). To deliver the granular carbonate to the region below the RPV, the delivery system must be able to pump or inject the granules. The density of the granules ranges from 2.7 to 3.0 g/cc (density of carbonates). In comparison, grains of rice have densities of 1.5 g/cc. So, the mass of carbonate is about twice the size of the rice grain. For a carbonate diameter of 2 cm, the volume is 4.19×10^{-6} m^3 and a mass of 0.011 kg (11.3 g). Therefore, it is possible that an agricultural type conveyer system could be used for delivering the carbonate granules.

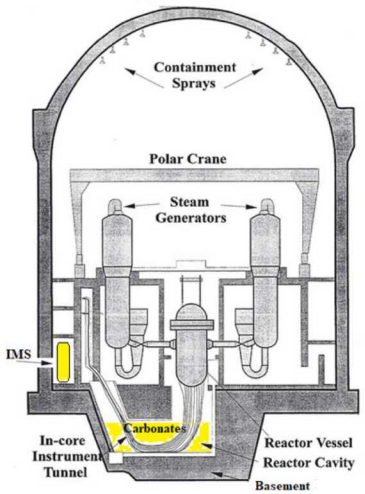

Fig. 1. Example of placing IMS and a carbonate bed in a PWR large dry containment

Commercial type conveyer systems for grain harvest may be used for delivering the carbonate granules at

centimeter range size. Similar size granules may use other systems [3]. Many of these conveyer systems use a screw type delivery system rather than a belt system. The typical diameter of the screw type conveyer system ranges from 15.24 cm to 33.02 cm [4]. The length of the conveyer could be from 7.62 m to 21.64 m. Volumetric flow could range from 1,600 bushels per hour (56.63 m^3 per hour) to 7,800 bushels per hour (276.08 m^3 per hour). Because these conveyer systems are used in agricultural applications, the cost associated with them is low. Since the availability of carbonate granules (limestone stone minerals) are vast, the only cost is to grind them into manageable sizes for injection. Because these mineral rocks do not require additional chemistry control measures, in contrast to the need for corrosion control in water-based systems, the maintenance associated an engineered system utilizing carbonate rocks is very low. A significant cost would be the modifications required to the containment boundary that would allow for a pathway to be established through which the carbonate could be injected into containment.

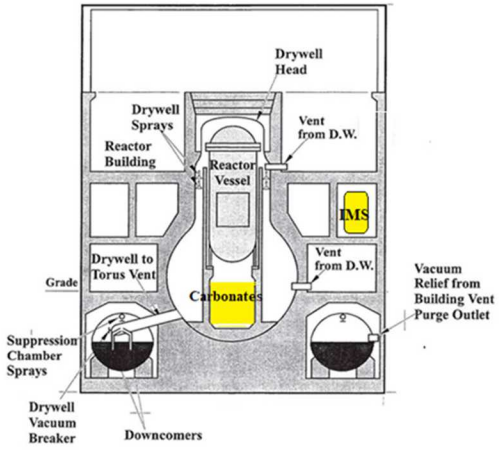

Fig. 2 Example of placing IMS and carbonate bed in a BWR Mark I containment

II.C. MCO3 Decomposition Model

A simplified carbonate decomposition model for a spherical particle of MCO3 with a reacted outer region and unreacted inner region surrounded by the melt (liquid corium) [3] has been developed, which is derived using a commonly known "shrinking core model" (SCM) [5]. The decomposition reaction of an alkaline carbonate is given below:

$$MCO_3 \xrightarrow{\mathcal{R}} MO + CO_2(g) + \Delta H \tag{1}$$

Where $\mathcal{R}$=mole reaction rate per unit area, ΔH=reaction energy in J/mol and M is the alkaline metal. $\mathcal{R}$ is given below:

$$\mathcal{R} = k(P_e - P) \tag{2}$$

Where k=reaction rate constant, P is the pressure at the unreacted MCO_3 surface, and P_e=equilibrium pressure of CO_2. Both k and P_e are given below:

$$k = k_0 e^{-\frac{\Delta E_R}{RT}} \tag{3}$$

$$P_e = P_e^0 e^{-\frac{\Delta H}{RT}} \tag{4}$$

k_0=referenced reaction rate constant, ΔE_R=the activation energy constant, P_e^0 =referenced equilibrium pressure for CO_2 and R=the gas constant.

T in Eq. (3) and (4) is the temperature at the unreacted MCO3 particle with an initial unreacted radius, r_0 and is given by:

$$T = T_m - \frac{\mathcal{R} \cdot \Delta H \cdot r_0 f^{1/3}}{\lambda}\left(1 - f^{1/3}\right) \tag{5}$$

Where T_m= melt temperature, λ=thermal conductivity of the oxide layer (MO), and f= ratio of unreacted over the initial MCO3 mass (m_0).

P in Eq. (2) is the unreacted MCO3 region and is given by:

$$P = P_m + \frac{R \cdot T \cdot \mathcal{R} \cdot r_0 f^{1/3}}{D}\left(1 - f^{1/3}\right) \tag{6}$$

Where P_m= melt pressure, which is the gas pressure above the melt and D= diffusion of CO_2 from the reaction surface and is given:

$$D = D_0 e^{\alpha T_s} \tag{7}$$

Where D_0= referenced diffusion coefficient, α=an exponent constant, and T_s=average temperature of T_m and T for simplicity. A more accurate correction for T_s is given in [3].

Considering a MCO3 bed with all same size particles and a porosity, ε, then, the MCO3 mass consumption rate is given by:

$$\frac{dm}{dt} = -(1-\varepsilon)\nu_{MCO_3}\mathcal{R} \cdot \frac{3f^{2/3}}{r_0} m_0 \tag{8}$$

Where ν_{MCO_3}= specific molar volume of MCO3. Then the heat loss from the melt, $\frac{dQ_{heat}}{dt}$ and molar generate rate, $\dot{M}$ of CO_2 are given below:

$$\frac{dQ_{heat}}{dt} = \frac{dm}{dt}\left(\frac{\Delta H}{\mathcal{M}} + C_p(T - T_0)\right) \tag{9}$$

$$\dot{M} = -\frac{1}{\mathcal{M}}\frac{dm}{dt} \tag{10}$$

Where $\mathcal{M}$=molecular weight and C_p=heat capacity of MCO3, and T_0=initial temperature of the MCO3.

In using the SCM above, the calculation needs to provide both T_m and P_m, and the model will update both m and P where P accounts for the gas pressure above the melt. Later in this paper, we apply this model in a full plant simulation to demonstrate the effect of the carbonate cooling.

III. MCO3 EXPERIMENTS USING PBO

To test the cooling capability of the MCO3 (SM) in the molten liquid, such as corium, lead oxide (PbO) was selected as the surrogate corium melt. PbO density is very close to that of UO_2 and the melting temperature of PbO is in the order of 1000 K to comply with environmental, safety, and health guidance at Sandia. We conducted both small-scale and large-scale tests using grams to a kilogram of PbO, respectively.

III.A. Small-Scale Tests

Over 30 benchtop sets of SM-melt interaction experiments have been conducted with different SMs (i.e., calcite, dolomites, pure CaCO3, $MgCO_3$ and PbO masses [3]. SM-melt experiments using molten PbO are poured onto a petri dish filled with MCO3 demonstrated the proof-of-principle. In each test, a certain quantity of PbO was first melted at ~ 1250 K. The melt was then poured into a silica dish containing a known amount of MCO_3. The temperature change and the extent of melt solidification were monitored in real time using a remote temperature gun and video camera. Post-experimental testing was performed to determine microstructures, chemical composition variations, and CO_2 bubble distributions in the resulting solidified materials. Then weight loss measurement was conducted to determine the amount of carbonate being decomposed as a function of the PbO mass interacted. Based on the microstructure identified from the experiments, such as open pore structures, a water volume measurement was conducted on a sample to determine the porosity of the open pore structure.

One test used $CaCO_3$ powders in a petri dish preheated at 823 K, molten PbO at 1248 K was poured on the dish. After cooling, the porosity of the open pore structure was measured using a water displacement technique. As shown in Fig. 3, the sample has a large opening on the top. Based on this technique, we calculated the bulk density. Finally, we examined this bulk density with pure density of PbO density to calculate the porosity. Since any by-product oxide and CO_2 trapped in the samples was negligible, the bulk porosity was about 70%.

The 4B test is similar to the above 1E test, except without preheating. The micro bubble structures and the sample after pour and cool are shown in Fig. 4. As shown in this Fig. 4 (a), swelling is observed due to build-up of CO_2 through the melt while it is solidifying. The distributions of the micro bubbles are shown in Fig. 4 (b) to (d). As shown in (b), the bubbles are concentrated near the surface of the sample, which suggests a convective flow along the surface of the sample during solidification. The larger bubbles tend to concentrate near the top of the sample. This action allows open pores to develop near the top of the surface as evidenced in this Fig. 4 (b) and Fig. 3. As shown in Fig. 5, the convection created a density inversion at the surface of the melt while it solidified. Note these observations of the structures were similar to those observed in the COMET spreading experiment [6].

Fig. 3 1E Test Sample used in the porosity determination

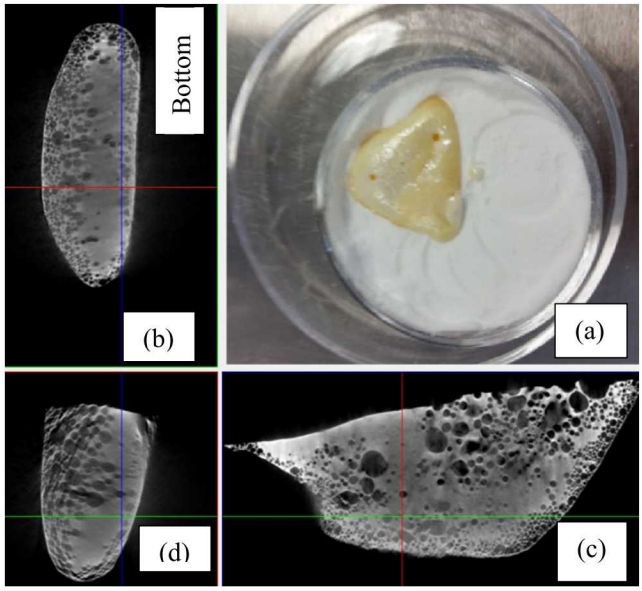

Fig. 4 4B Test Sample: (a) after pour and cool, (b) to (d) are the X-ray micro CT imaging of the micro bubbles in the sample

Fig. 5 5F Test sample (dolomite) after cool

III.B. Large-Scale Tests

To verify scalability from the small-scale tests, many large-scale confirmatory tests were performed using about 1 kg of PbO. A tube furnace with a containment tube (made of alumina) and a crucible tube holding the PbO were used. Fig. 5 shows the apparatus for the large-scale tests. As shown in this figure, the tube furnace is mounted on a crank shaft with a hand crank. The tube is pointed upward as shown in this figure while the PbO is melting. When the melt reaches a desired liquid temperature (i.e., about 1273 K), the crank shaft is turned to pour PbO melt into the catch pan where the sand or carbonate bed is located. Several thermocouples are wired in the pan and in and around the furnace to detect the temperature response. During the early part of the testing, several failures due to chemical incompatibility between the heating tube and PbO, and thermal shock were encountered. A detail of the issues is given in [3]. The large-scale pour tests further confirm the experimental results obtained from the small-scale tests that the endothermic reaction of an alkaline carbonate mineral can effectively remove the heat from PbO melt and lead to a quick solidification of the melt. The solidified PbO is porous and contains multiple-scale pores (Fig. 6). These pores are formed by the bubbling of CO_2 gas released from carbonate decomposition. Vigorous convection and mixing were observed during the PbO melt-carbonate mineral interaction. The convection and mixing were driven by the density inversion in the system as well as by CO_2 degassing.

Fig. 5 Apparatus of a tube furnace connected to a crank for pouring onto a catch pan

(a) pour (b) after cool

Fig. 6 Test 7 with PbO onto Calcites

III.C. CFD Model for Experiments

Sandia's Sierra/Aria CFD code was used to simulate the PbO-MCO3 interaction. The modeling approach is similar to the methods described in [3, 7]. The lead oxide numerical experiments were conducted in two dimensions to simplify the analysis. The initial condition and mesh for these experiments are shown in Fig. 7. An unstructured mesh of triangular P1 elements is used as the background mesh, with a finer mesh near the quartz substrate, representing the dish (shown in yellow). The conformal interface between the air (green) and lead-oxide (blue) phase generated by the conformal mapping method employed in the confirm decomposition infinite element method is clearly shown. As the conformal interface moves, the mesh will "conform" to this interface, allowing us to introduce boundary conditions explicitly on the air/lead-oxide interface such as surface tension and convective/radiative heat losses.

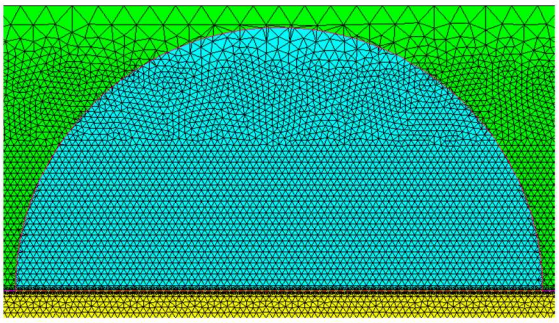

Fig. 7 Initial condition and mesh for the benchtop lead-oxide experiment. Blue represents the lead oxide phase, green is the air phase, and yellow is the quartz substrate

Several equations are solved in this system in a segregated manner. The equations solved are the incompressible Navier-Stokes equations and energy equation given as

$$\nabla \cdot \mathbf{u} = 0 \tag{11}$$

$$\rho\left(\frac{\partial \mathbf{u}}{\partial t} + \mathbf{u} \cdot \nabla \mathbf{u}\right) = -\nabla p + \nabla \cdot \left(\mu(\nabla \mathbf{u} + \nabla \mathbf{u}^{\mathbf{T}})\right) \tag{12}$$

$$\rho C_p \left(\frac{\partial T}{\partial t} + \mathbf{u} \cdot \nabla T\right) - \nabla \cdot (k \nabla T) = \dot{q} \quad (13)$$

where $\boldsymbol{u}$ is the velocity vector, ρ is the density, p is the pressure, μ is the viscosity, T is the temperature, k is the thermal conductivity, C_p is the specific heat, and q is the heat source scalar. All these material properties are a function of the phase of the material, which is given by the level set equation

$$\frac{\partial \phi}{\partial t} + \mathbf{u} \cdot \nabla \phi = 0 \quad (14)$$

where ϕ represents the level set field and is defined as the signed distance function to the air/lead-oxide interface, which is the level set zero. Depending on the sign of the signed distance function, the material property will assume either the lead-oxide or air phase. For instance, in Fig. 7, the blue phase represents the negative level set field ϕ, and is the lead-oxide phase. Therefore, the properties in Eq. 11 to Eq. 13 (density, specific heat, etc.) are that of the lead-oxide phase. The air phase properties are used for the positive level set field (green in Fig. 7). The velocity obtained from solving the momentum equations (Eq. 11 to 13) are advected to the level set Eq. 14, where $\phi = 0$ defines the interface where the conformal mapping is used to cut the elements. Because Eq. 14 does not maintain ϕ as a distance function, the level set needs to be periodically re-distanced. Mass conservation is also an issue and a constraint is added to reduce mass loss or gain during distancing.

Surface tension is applied at the interface through the following boundary condition

$$[-p\mathbf{I} + \mu(\nabla \mathbf{u} + \nabla \mathbf{u}^T)]_\Delta \cdot \mathbf{n} = -\gamma \kappa \mathbf{n} \quad (15)$$

where $\boldsymbol{n}$ represents the surface normal on the interface, κ is the interface curvature, γ is the surface tension, and $[\cdot]_\Delta$ represents a jump of the bracketed expression across the interface. The total stress is discontinuous in the normal direction across the interface and proportional to the surface curvature. In the absence of viscous stresses, this equation reverts to the familiar balance between the capillary pressure and surface tension across a curved interface.

Conjugate heat transfer between the air and lead-oxide is not explicitly modeled, and instead is modeled through a convective heat flux boundary condition given as

$$q_{conv} = h(T - T_{ref}) \quad (16)$$

where T_{ref} is the ambient air temperature and h is the convective heat transfer coefficient. Thermal radiation is also included.

Surface tension and convective/radiative models are employed at the air/lead-oxide interface, along with a constant hydrostatic force (gravity) in the y-direction. Thus, the spreading of the lead oxide will occur through the combination of these forces, where gravity, surface tension, and a cooling interface through convection and radiation (which then solidifies the melt using the Ramacciotti viscosity model [7]) will dictate the spreading rate and final shape of the lead oxide.

To model the slip of the contact line between the air/lead-oxide/quartz (green/blue/yellow phases in Fig. 7, we use the Navier-slip boundary condition on the lead-oxide/quartz surface

$$u_{slip} = \beta \frac{\partial u}{\partial n} \quad (17)$$

where β is the "slip length". The selection of this slip length can be somewhat arbitrary, and as $\beta \to 0$ the no-slip condition can be recovered for infinite shear stress at the boundary. Simply, the lower the value of the slip length β, the more stress that must exerted on the fluid/solid boundary to initiate (or continue) motion.

To simulate the reaction of $CaCO_3$ with PbO, we leveraged the general chemistry modeling capabilities of Aria [3]. The calcium carbonate is heated from room temperature by the molten lead-oxide and thereby releases CO_2 gas and solid CaO. This reaction rate is evaluated through an Arrhenius model. The activation energy in the model was fitted from the thermo-gravimetrical analysis of the experiments [3]. Consequently, a species transport equation is also solved as part of the segregated equation system

$$\frac{\partial C_k}{\partial t} + \boldsymbol{u} \cdot \nabla C_k = -\nabla \cdot \boldsymbol{J}_k + R_{V,k} \quad (18)$$

where C_k is the concentration of species k, $\boldsymbol{J}_k$ is the molar flux (Fick's law is used to approximate this), and $R_{V,k}$ is the volume source of species k, which is obtained from solving a system of ordinary differential equations for the reaction rate derived from the reaction defined and Eq. 18.

Additionally, the volumetric reaction rate $\dot{q}$ is calculated as

$$\dot{q} = \sum_{j=1}^{N_r} \Delta H_{rxn,j}\, r_j \quad (19)$$

where N_r is the number of reactions (in this case, one) and r_j is the calculated reaction rate of a specific reaction j, which is obtained from solving the system of reaction ordinary differential equations described earlier. This provides a coupling between the chemistry reactions and the endothermic energy release of the calcium carbonate as it meets the hot lead oxide.

To use the above model, we model a petri dish with a diameter of 9 centimeters with a very thin concentration of calcium carbonate on the bottom, corresponding to approximately 0.5 grams of material. A hemispherical shaped mass of lead oxide, corresponding to approximately 20 grams of material, is introduced into the simulation as an initial condition. An image of the initial shape of the lead

oxide and calcium carbonate concentration is shown in Fig.8. In this figure, the calcium carbonate is concentrated in a thin layer above the petri dish (yellow). Not pictured here is that this thin layer extends to within the lead oxide mass. This was done for ease of computation. In future work, it might be beneficial to start with more of a droplet shape, or to introduce the mass from the air and allow it to splash into the dish. However, the purpose of this exercise was to investigate the interaction of the lead oxide with the calcium carbonate through the general chemistry coupling in Aria, so keeping a simple initial state is imperative.

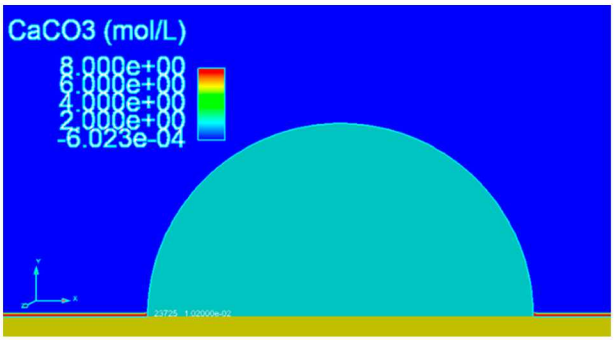

Fig. 8 Initial configuration of the lead oxide (teal) and concentration of the calcium carbonate layer (red).

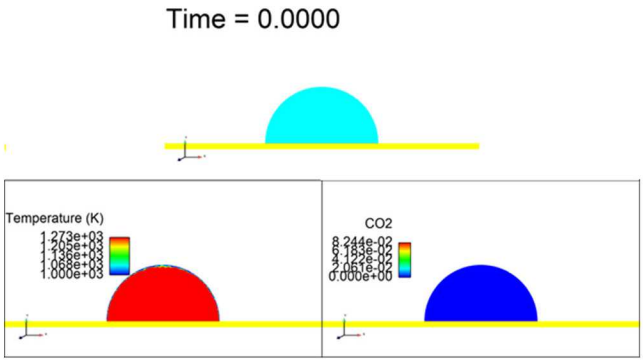

Fig. 9 Initial configuration. Top, colored by phase (teal lead oxide); bottom left, colored by temperature; bottom right, colored by concentration of CO_2

The initial PbO temperature was 1,273 K. The PbO is then free to spread along the plate, as shown in 0 and 0.53 second time images in Fig. 9 and Fig. 10, respectively. The reader should refer to [3] for more results. The reaction is quite rapid and was set to complete when all the calcium carbonate has been consumed (concentration goes to zero). As time goes on, the melt has begun to spread and reacts with the calcium carbonate, lowering the temperature near the interface with the calcium carbonate. CO_2 is also being produced as a byproduct which is not shown in these figures. In Fig. 10, after 0.53 seconds, the system is approaching a steady state as CO_2 continues to diffuse into the material. It has also advected somewhat while the melt was moving at earlier times, as evidenced by the increased concentration toward the edges of the lead oxide melt. At this time, the radiative and convective cooling has begun to solidify the outer portions of the material that did not meet the calcium carbonate at any point.

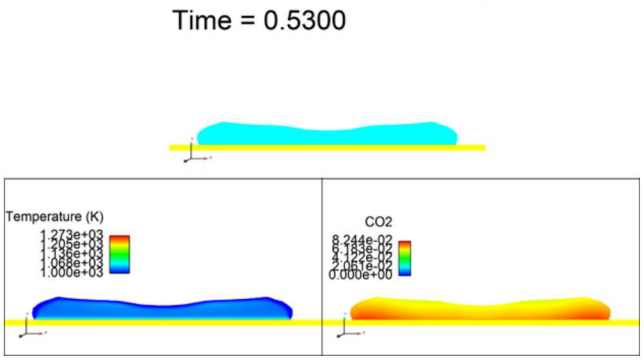

Fig. 10 Time of 0.53 seconds. Top colored by phase (teal lead oxide); bottom left, colored by temperature; bottom right, colored by concentration of CO_2

Fig. 11 shows the melt front position as a function of time. The front ceases to advance after about 0.1 seconds, indicating a rapidly cooling lead oxide front as it reacts with the calcium carbonate layer. While we were unable to replicate the "loafing" behavior seen in the small-scale experiments, the alacrity at which the lead oxide has solidified is impressive. This rapid solidification would not have occurred through convective radiative heat losses, or even through conduction with the quartz petri dish. These results seem nominally "correct" compared to the benchtop experiments and with further model development, we will include loafing and other effects, such as density inversion and bubble distribution as observed in the experiments.

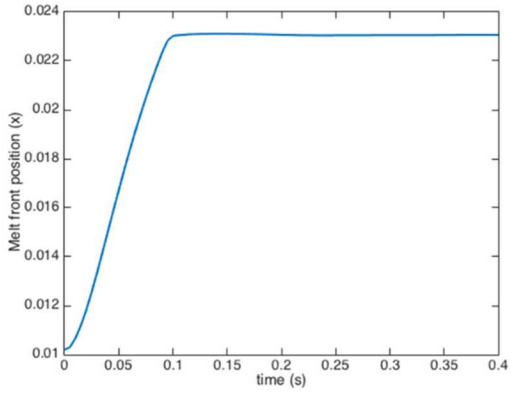

Fig. 11 Melt front position (x) vs. time (s); melt front does not continue to advance after 0.1 seconds

IV. MELCOR SIMULATION

To investigate the potential benefits of introducing the carbonate granules to the reactor cavity/pedestal area in a severe nuclear reactor accident, two MELCOR calculations were performed. We used a BWR-4 Mark I MELCOR deck. The accident scenario was a long-term station blackout (LTSBO) affecting the BWR-4 reactor situated in a Mark I containment. The base case does not include carbonate granules. The second calculation is made by adding a large quantity of carbonate materials (using $CaCO_3$) as SM into the pedestal (drywell) region below the RPV as a postulated accident mitigation measure. In this second calculation, a representation (the SCM representation described in Section II. C) of the cooling reaction that would take place between core debris on the containment floor and SM situated on the floor prior to failure of the RPV lower head. The parameters used in the SCM included the assumed carbonate particle size of 0.01m, bed porosity of 0.4, thermal conductivity of CaO of 7 W/m-K, and α=0.0165 K^{-1} Eq. 7 (see [3] for more details). An SM mass of 280 metric tons was sourced onto the pedestal before RPV lower failure, which is based on Table II for Mark I BWR.

To illustrate the accident sequences of these two cases, an event table is presented in Table III. As shown in this table, the sequence of events for both with and without SM injection is the same up to the point when the RPV fails to allow molten corium to relocate onto the pedestal floor below the RPV. Note that this sequence was chosen as an illustration of the SM cooling. The failure of RCIC due to turbine flooding would not affect the outcome. It is assumed in the SM simulation that the carbonate remains at T_0 of 295 K in Eq. 9. In reality, after the injection, the temperature of the SM bed may rise to the ambient temperature of the pedestal, which could absorb the heat from the surrounding before the RPV fails. As shown in this table, the early sequences are identical up to the RPV lower head failure for both cases. The reader is encouraged to read about the early part of the sequences in [3]. In this paper, we describe the differences in the results for the cases with and without SM. As shown in Table IV, with SM in place, the severity of the accident is delayed at least > half a day. which may be enough for additional accident management to alleviate the situation.

Fig. 12 shows the containment pressure comparison, which indicates a large difference, reflecting core debris spreading on the containment floor to the containment liner and melting through the liner much earlier in the case without SM reaction. The containment depressurizes through the breach in the liner. Important to realize in considering the pressure response in the calculations, is that leakage at the drywell head flange is modeled and that the leakage effectively regulates maximum pressure.

Fig. 13 compares the core debris temperature in in the reactor cavity (on the containment floor beneath the reactor). The cooling influence of SM reaction is clear in this figure. The peaks shown in this figure reflects the core-concrete interaction. Fig. 14 is a comparison of the molar concentration of both CO and H_2 produced relative to all gas produced from in-vessel oxidation, core-concrete interaction and SM reaction. The figure shows that the SM reaction in a severe accident reduces relative CO and H_2 concentrations and thereby effectively reduces the CO and H_2 ignition potential. Both cases saw debris reaching the liner but with substantially different timing. Debris reaching the liner was assumed to melt through the liner in simulations, breaching containment. However, the SM provided almost 15 hours for additional actions to prevent the containment liner failure.

TABLE III

MELCOR calculations key event timing for Mark I BWR LTSBO with/without SM Injection [3]

Event	Timing (hr:min:sec)	
	Without SM	With SM
Loss of all alternative current (AC) power	00:00:00	00:00:00
Main steam isolation valves (MSIVs) close	00:00:00+	00:00:00+
Reactor scram	00:00:00+	00:00:00+
Reactor core isolation cooling (RCIC) system starts on low level	00:10:19	00:10:19
Operators initiate 100 °F/hr cooldown (safety relief valve (SRV) opened, RCIC throttled)	01:00:00	01:00:00
SRV closes on battery depletion	04:00:00	04:00:00
RCIC turbine floods failing RCIC	5:53:37	5:53:37
Downcomer level drops to the top of active fuel	8:29:52	8:29:52
First fuel-cladding gap release	9:31:39	9:31:39
Cycling SRV fails to reclose	NA	NA
MSL rupture	12:03:37	12:03:37
Drywell head flange leakage begins	12:04:12	12:04:12
Reactor building (refueling bay) blow-out panels blow out	12:05:08	12:05:08
First large-scale relocation of core debris to lower plenum	12:40:27	12:40:27
RPV lower head dry	13:10:54	13:10:54
RPV lower head failure	18:37:56	18:37:56
SM reaction begins	NA	18:38:00
Core-concrete interaction begins	18:37:57	33:15:00
Drywell liner melt-through	19:46:21	37:37:54
SM consumed	NA	34:05:00
H_2 burns initiate in reactor building grossly damaging the building	19:46:42	37:38:39

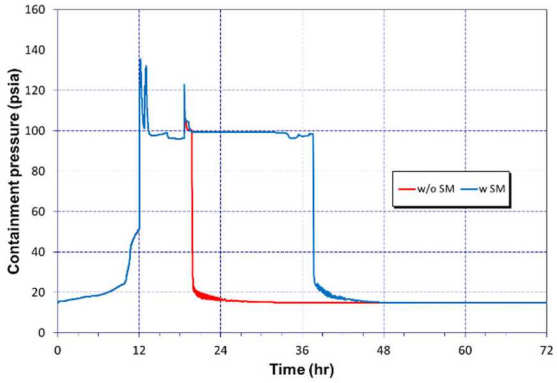

Fig. 12 Containment pressure comparison

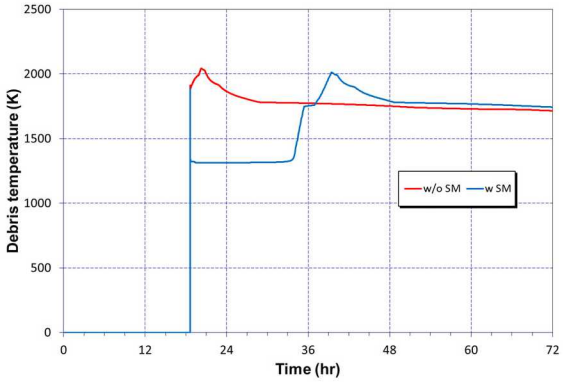

Fig. 13 Core debris temperature comparison

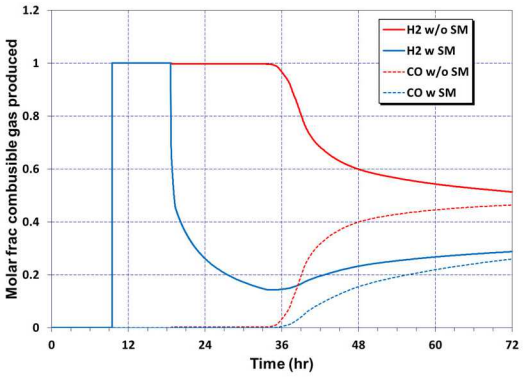

Fig. 14 Combustible gas molar fraction comparison

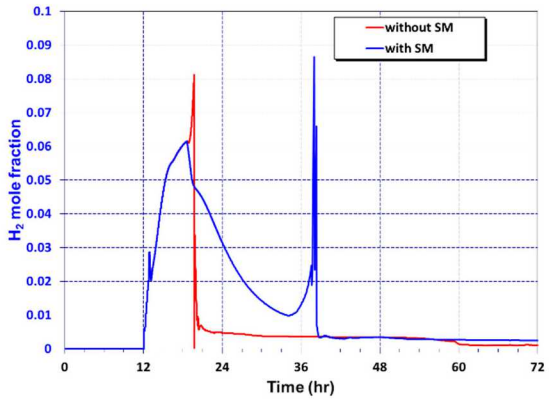

Fig. 15 Comparison of refueling bay H_2 concentration

Following the liner failure, the containment blew down into the reactor building. The blowdown caused H_2 concentration to spike in the building as shown in Fig. 15 and reach a burnable concentration. The H_2 ignited, which is expected to cause gross building damage that will significantly hamper subsequent mitigation efforts.

IV. CONCLUSIONS

In this paper, the use of alkaline carbonate as SM in particulate form can be injected into the cavity or pedestal in the PWR and BWR plant to mitigate the ex-vessel molten corium as the IMS. The interaction with melt (PbO) experiments in this research has demonstrated that the resulting solidified melt contains open pore structures by the generation of CO_2 from the endothermic decomposition of the alkaline carbonate. If the IMS is deployed to mitigate the ex-vessel corium accident, the material cost and delivery system are very low. A significant cost would arise from modifications to the containment boundary to allow for a pathway to be established for injecting the carbonate. Also, this research has shown that the severity of the accident can be delayed more than ½ day, which permits the resulting cooled corium solid contains open pore structures to be effectively cooled by subsequent water injection during the recovery period. The re-melt may not be possible if adequate water is provided. The generation of CO_2 can also reduce the likelihood of the hydrogen gas explosion.

ACKNOWLEDGMENTS

This paper describes objective technical results and analysis. Any subjective views or opinions that might be expressed in the paper do not necessarily represent the views of the U.S. Department of Energy or the United States Government. Sandia National Laboratories is managed and operated by National Technology and Engineering Solutions of Sandia, LLC for U.S. DOE/NNSA under contract DE-NA0003525. This research was supported by the

Laboratory Directed Research and Development Program of Sandia National Laboratories. The authors like to thank K.C. Wagner of Sandia for reviewing this paper.

NOMENCLATURE

AC	Alternating current
AFW	Auxiliary feed water
BWR	Boiling water reactor
IR	Infrared
LDRD	Laboratory directed research and development
LTSBO	Long-term station blackout
LWR	Light water reactor
MSIV	Main steam isolation valve
PWR	Pressurized water reactor
RCIC	Reactor core isolation cooling
RCS	Reactor cooling system
RPV	Reactor pressure vessel
SM	Sacrificial material
Sandia	Sandia National Laboratories
SRV	Safety relief valve
TC	Thermocouple
TD	Turbine driven
TGA	Thermo-gravimetrical analyses
C_k	Concentration of species, k
C_p	Heat capacity
D	CO_2 diffusion coefficient
D_0	Initial CO_2 diffusion coefficient
f	Fraction of the initial radius or mass of the unreacted carbonate from initial value
k	Reaction rate constant, thermal conductivity
k_0	Initial reaction rate constant
MCO3	Alkaline carbonate
$\dot{M}$	Molar rate
$\dot{m}_{prod}$	Reaction production rate
$\boldsymbol{n}$	Surface normal on interface
P	Pressure at the unreacted carbonate surface
P_0	Initial unreacted carbonate pressure
P_e	Equilibrium pressure of CO_2
P_e^0	Initial equilibrium pressure of CO_2
P_m	Melt pressure
p	pressure
$\dot{q}_{heat}$	Heat removal rate by the particle
q_{conv}	Convective heat flux
R	Gas constant
r	Radius of the carbonate particle
r_0	Initial of the unreacted carbonate particle
T	Temperature of the unreacted carbonate
T_l	Liquidus temperature
T_m	Melt temperature
T_{ref}	Ambient air temperature
T_s	Interface temperature between melt and unreacted carbonate, solidus temperature
t	Time
$\boldsymbol{u}$	Velocity vector
u_{slip}	Slip velocity
α	Exponent constant for CO_2 diffusion
β	Slip length
ε	Bed porosity
ΔE_R	Activation energy constant
ΔH	Specific reaction energy per mole
ΔH_{rxn}	Heat of reaction
λ	Thermal conductivity of oxide layer
$\mathcal{M}$	Molecular weight
$\mathcal{R}$	Reaction rate
ϕ	One minus bed porosity
ν	Specific volume

REFERENCES

1. Sehgal, E.R., Nuclear Safety in Light Water Reactors: Severe Accident Phenomenology, Academic Press, Elsevier, 2012

2. Komley, S., et al., "New Sacrificial Material for Ex-Vessel Core Catcher," Journal Nuclear Materials, **467**, pg. 778-784, 2015.

3. Louie, D.L.Y., et al., A New Method to Contain Molten Corium in Catastrophic Nuclear Reactor Accident, SAND2019-13133, Sandia National Laboratories, October 2019.

4. http://www.grainaugers.com/products/straight-augers/wr-w-series, AGI Westfield, 2019.

5. Stanmore, B.R. and Gilot, P., "Review-Calcination and Carbonation of Limestone During Thermal Cycling for CO2 Sequestration," Fuel Processing Technology, **86** 1707-1743, 2005.

6. Alsmeyer, H., and Tromm, W., The COMET Concept for Cooling Core Melts: Evaluation of the Experimental Studies and Use in the EPR, FZKA 6186, EXV-CSC (99)-D036, Institut fur Kern- und Energietechnik, Forschungszentrum Karsruhe GmbH, Karlsruhe, 1999.

7. Kucala, A., et al., "A Computational Model for Molten Corium Spreading and Solidification," Computers & Fluids, **178**, 15, pg.1-14, January 2019.